Letter

Terahertz spin-light coupling in proximitized Dirac materials

Konstantin S. Denisov,[1,2,*] Igor V. Rozhansky,[1] Sergio O. Valenzuela,[3,4] and Igor Žutić[2]

[1]*Ioffe Institute, 194021 St. Petersburg, Russia*

[2]*Department of Physics, University at Buffalo, State University of New York, Buffalo, New York 14260, USA*

[3]*Catalan Institute of Nanoscience and Nanotechnology (ICN2), CSIC and BIST, Bellaterra 08193, Spain*

[4]*Institució Catalana de Recerca i Estudis Avançats (ICREA), Barcelona 08010, Spain*

(Received 1 June 2023; revised 1 November 2023; accepted 25 April 2024; published 16 May 2024)

The two-dimensional (2D) materials are highly susceptible to the influence of their neighbors, thereby enabling the design by proximity phenomena. We reveal a remarkable terahertz (THz) spin-light interaction in 2D Dirac materials that arises from magnetic and spin-orbital proximity effects. The dynamical realization of the spin-charge conversion, the electric dipole spin resonance (EDSR), of Dirac electrons displays distinctive THz features upon emerging spin-pseudospin proximity terms in the Hamiltonian. To capture the effect of fast pseudospin dynamics on the electron spin, we develop a mean-field theory and complement it with a quantum-mechanical treatment. As a specific example, we investigate the THz response of a single graphene layer proximitized by a magnetic substrate. Our analysis demonstrates a strong enhancement and anomalous polarization structure of the THz-light absorption, which can enable THz detection and efficient generation and control of spins in spin-based quantum devices. The identified coupled spin-pseudospin dynamics is not limited to EDSR and may influence a broad range of optical, transport, and ultrafast phenomena.

DOI: 10.1103/PhysRevB.109.L201406

Heterostructures combining two-dimensional (2D) van der Waals (vdW) materials offer innovative approaches for tailoring material properties [1,2]. The atomically thin 2D layers imply that many phenomena can be dominated by proximity effects [3,4]. This scenario is exemplified in spin-dependent properties of graphene-vdW heterostructures [3–7]. Transition metal dichalcogenides imprint spin-pseudospin-valley splitting and spin-orbit coupling (SOC) onto graphene [4,8–11], leading to spin filtering [12–14] as well as enhanced spin-to-charge interconversion [15–19]. An exchange field and ensuing carrier spin splitting can be further induced in graphene through magnetic proximity [20–25].

These added functionalities can pave the way to novel topological phases and devices that merge spin injection, detection, and manipulation into a single graphene platform [4,7,26]. Graphene and other Dirac materials have a great potential for THz (opto)electronics. Fast, room-temperature THz detectors made of graphene exhibit excellent sensitivity, high dynamic range, and broadband operation [27]. Massless Dirac fermions in graphene and topological insulators have large nonlinear optical coefficients and harmonic conversion efficiencies, suitable for THz high-power harmonic generation [28–30].

In this work, we investigate the spin-charge THz dynamics in proximitized 2D Dirac material with spin splittings, as shown in Fig. 1, and describe the resulting spin-light interaction including SOC. Our results demonstrate an unexplored realization of the spin-charge conversion from the electric dipole spin resonance (EDSR) [31,32], the excitation of electron spin precession by an ac electric field, which is a versatile tool from probing SOC, inhomogeneous magnetism, and topological states to realizing spin injection and controlling qubits [33–43]. In the presence of SOC, the EDSR is driven by a unique mechanism due to coupled spin-pseudospin dynamics [44,45]. Previously overlooked, this phenomenon becomes crucial at frequencies ω in the THz range, where $\omega\tau_p \gg 1$, with τ_p the momentum relaxation time. We calculate the absorption in proximitized graphene, using realistic SOC and magnetic exchange parameters, and demonstrate that the predicted EDSR leads to a remarkable increase of both the spin susceptibility and THz absorption. We reveal an anomalous polarization structure of EDSR controlled by the coupled spin-pseudospin dynamics and transformed for massive Dirac electrons upon lowering the Fermi energy, μ. Our findings (i) provide striking differences from prior mechanisms [37,38,46,47] and (ii) highlight their relevance for THz detection and spin manipulation.

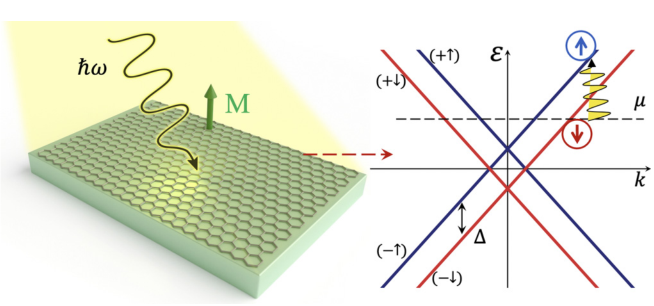

FIG. 1. Electric field of THz radiation causes intersubband spin-flip transitions in a graphene on a substrate with a magnetization, **M**. The Dirac spectrum with a proximity-induced spin splitting, **Δ**, wave vector, **k**, and the Fermi energy, μ.

*denisokonstantin@gmail.com

The electron spin resonance (ESR) [36,48] is a well-established technique for studying spin phenomena in solids. It requires a static magnetic field that defines the direction of an equilibrium spin polarization, ac-magnetic field, that induces spin-flip transitions, which are detected by the absorption close to the Larmor frequency. The EDSR is essentially identical, but with the spin-flip transitions induced by ac-electric field, allowed in the presence of SOC [31,32,49]. In nanostructures the SOC symmetry and magnitude can be designed to increase the efficiency of spin-flip absorption for a stronger spin-light interaction in the EDSR than in ESR. This is very desirable for semiconductor qubits [39,42,43] and to resonantly enhance the spin-charge conversion.

We analyze the EDSR for the low-energy Hamiltonian of Dirac electrons in a hexagonal system near the K and K' valleys, including magnetic exchange and SOC

$$\mathcal{H} = \mathcal{H}_0 + \mathcal{H}_{\rm ex} + \mathcal{H}_{\rm so}, \tag{1}$$

where $\mathcal{H}_0 = \hbar\boldsymbol{\Omega}_k \cdot \boldsymbol{\tau}$ defines the Dirac spectrum, $\hbar$ is the Planck constant, with $\boldsymbol{\tau}$ the lattice pseudospin operator [50], $\boldsymbol{\Omega}_k = 2v_F(\xi k_x, k_y, U/2\hbar v_F)$ the Larmor frequency, $\boldsymbol{k}$ the electron wave vector, v_F the Fermi velocity, and $\xi = \pm 1$ the valley index. In z component of $\boldsymbol{\Omega}_k$, U is the strength of the staggered potential, due to the on-site asymmetry between two inequivalent sublattices in 2D hexagonal lattices deriving from different atoms in the unit cell or from the effect of a substrate. $\mathcal{H}_{\rm ex} = \boldsymbol{\Delta} \cdot \boldsymbol{s}$ describes the magnetic exchange, where $\boldsymbol{s}$ is the spin operator, and Δ the spin splitting in the meV (THz) range [4], whereas $\mathcal{H}_{\rm so} = \hbar\boldsymbol{\Omega}_{\rm so}(\boldsymbol{\tau}) \cdot \boldsymbol{s}$ characterizes the SOC, where we assume a $\boldsymbol{k}$-independent $\boldsymbol{\Omega}_{\rm so}(\boldsymbol{\tau})$. For a graphene/TMD, $\mathcal{H}_{\rm ex}$ is the valley-dependent splitting $\xi\boldsymbol{\Delta} \cdot \boldsymbol{s}$.

A hallmark of Dirac materials is the spin-pseudospin coupling and their entanglement [4,10,44,45] arising from $\mathcal{H}_{\rm so}$. To model the spin-pseudospin dynamics driven by an electromagnetic wave, we consider the interaction $\mathcal{V} = \hbar\boldsymbol{\Omega}_{\rm int}(t) \cdot \boldsymbol{\tau}$, where $\boldsymbol{\Omega}_{\rm int} = -2(e/\hbar c)v_F(\xi A_x, A_y)$, with $\boldsymbol{A}$ the vector potential. At normal incidence, we focus on the spin-light coupling emerging via an electric field component $\boldsymbol{E}_\omega = (i\omega/c)\boldsymbol{A}_\omega$.

We describe the coupled spin-pseudospin dynamics by the mean-field equations of motion for the classical vectors $\boldsymbol{\tau}, \boldsymbol{s}$ [51]

$$\dot{\boldsymbol{\tau}} = ([\boldsymbol{\Omega}_k + \boldsymbol{\Omega}'_{\rm so}(\boldsymbol{s})] \times \boldsymbol{\tau}) + [\boldsymbol{\Omega}_{\rm int}(t) \times \boldsymbol{\tau}], \tag{2}$$

$$\dot{\boldsymbol{s}} = ([\boldsymbol{\Omega}_{\rm ex} + \boldsymbol{\Omega}_{\rm so}(\boldsymbol{\tau})] \times \boldsymbol{s}), \tag{3}$$

where $\boldsymbol{\Omega}'_{\rm so}(\boldsymbol{s})$ is obtained from $\mathcal{H}_{\rm so}$ by $\boldsymbol{\tau}\boldsymbol{\Omega}'_{\rm so}(\boldsymbol{s}) = \boldsymbol{s}\boldsymbol{\Omega}_{\rm so}(\boldsymbol{\tau})$ and $\hbar\boldsymbol{\Omega}_{\rm ex} = \boldsymbol{\Delta}$. For $\Omega_{\rm so} \lesssim \Omega_{\rm ex}$, this model captures the spin resonance at $\hbar\omega \approx \Delta$. $\boldsymbol{E}_\omega$ induces the dynamics of $\boldsymbol{\tau}$, which triggers the $\boldsymbol{s}$ precession due to spin-pseudospin coupling [44], as depicted in Fig. 2. For $\Omega_{\rm ex}\tau_p \gg 1$, the intersubband spin-light coupling results in a resonant absorption peak, as discussed below.

We provide our framework for n-doped graphene with $U = 0$; the case of $U \neq 0$ is given in [51] (see also Refs. [52,53] therein). The dynamics of two-level systems, including the lattice pseudospin, can be modeled using the classical precession equation for the quantum average of the operator, consisting of the corresponding Pauli matrices [54,55]. Ignoring SOC, Eq. (2) describes the free pseudospin oscillations with Ω_k and, when subjected to an external oscillating field

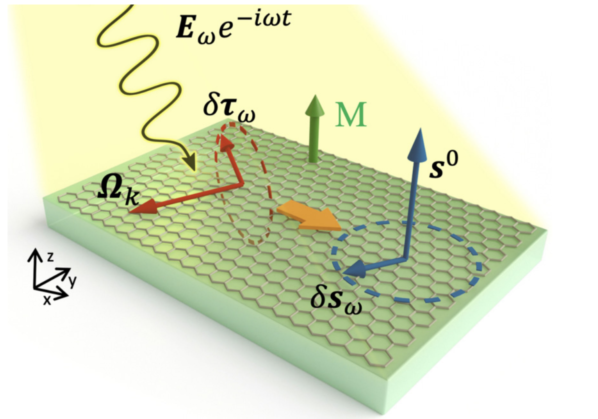

FIG. 2. EDSR of a Dirac electron driven by coupled spin-pseudospin dynamics. An incident THz radiation (yellow) with electric field $\boldsymbol{E}_\omega$ is absorbed creating a pseudospin component, $\delta\boldsymbol{\tau}_\omega$, which precesses in the pseudospin field, $\boldsymbol{\Omega}_k$, exerting a torque on a spin due to SOC (depicted by the orange arrow). Therefore, a spin component, $\delta\boldsymbol{s}_\omega$, precesses $\perp$ to the spin splitting $\boldsymbol{\Delta}$, which is along the equilibrium spin $\mathbf{s}^0$.

$\boldsymbol{\Omega}_{{\rm int},\omega}e^{-i\omega t}$, captures the resonance at $\omega \approx \Omega_k$, related to quantum pseudospin-flip transitions. An electron from the K valley with $\boldsymbol{k}$ has a static pseudospin $\boldsymbol{\tau}^0 = \hat{\boldsymbol{k}}/2$, parallel to $\boldsymbol{\Omega}_k = 2v_F\boldsymbol{k}$. Applying $\boldsymbol{\Omega}_{\rm int}(t)$ generates the torque $\boldsymbol{\Omega}_{\rm int}(t) \times \boldsymbol{\tau}^0 \propto \hat{\boldsymbol{k}} \times \boldsymbol{A}(t)$, which, following Eq. (2), triggers the pseudospin rotation around $\boldsymbol{\Omega}_k$. With $\boldsymbol{A}(t) = 2\,{\rm Re}[\boldsymbol{A}_\omega e^{-i\omega t}]$, the linear response $\delta\boldsymbol{\tau}_\omega = \delta\tau_z\hat{\boldsymbol{z}} + \delta\tau_\varphi\hat{\boldsymbol{\varphi}}$ is perpendicular to $\boldsymbol{\Omega}_k$

$$\delta\tau_{z,\varphi}(\omega) = \frac{\alpha_{z,\varphi}\mathcal{T}}{\Omega_k^2 - \omega^2}, \quad \mathcal{T} = e\frac{v_F}{\hbar c}[\boldsymbol{A}_\omega \times \hat{\boldsymbol{k}}]_z, \tag{4}$$

where $\alpha_{z,\varphi} = (-i\omega, \Omega_k)$. Poles in $\delta\tau_{z,\varphi}(\omega)$ at $\omega = \Omega_k$ give the pseudospin resonance, i.e., the interband transitions leading to the universal absorption $\alpha_0 = \pi\, e^2/\hbar c$. To obtain the interband absorption $\alpha = (\alpha_0/2)[\Theta(\hbar\omega - 2\mu + \Delta) + \Theta(\hbar\omega - 2\mu - \Delta)]$, Θ being the Heaviside function, one further needs to calculate the real part of the conductivity by summing $2v_F\delta\tau_\varphi(\omega + i0)\hat{\boldsymbol{\varphi}}_x$ over all quantum numbers with the equilibrium distribution function [51].

To illustrate the spin-pseudospin dynamics, we consider surface inversion asymmetry and the relevant Bychkov-Rashba SOC [56,57]

$$\mathcal{H}_{\rm so} = 2\lambda_{\rm so}(\xi\tau_x s_y - \tau_y s_x), \tag{5}$$

where the SOC strength $\lambda_{\rm so} \lesssim \Delta$ [3,4,22]. For the spin dynamics, in the lowest order of $\lambda_{\rm so}/\mu$, we account for $\mathcal{H}_{\rm so}$ only in Eq. (3). The oscillating pseudospin, $\delta\boldsymbol{\tau}(t) = 2\,{\rm Re}[e^{-i\omega t}\delta\boldsymbol{\tau}_\omega]$, induced by $\boldsymbol{E}_\omega$, then contributes to $\hbar\boldsymbol{\Omega}_{\rm so}(t) = 2\lambda_{\rm so}[\hat{z} \times \delta\boldsymbol{\tau}(t)]$ and exerts a torque on $\boldsymbol{s}$ (Fig. 2). For the out-of-plane geometry, $\boldsymbol{s}^0 \parallel \boldsymbol{\Delta} \parallel \hat{z}$, the resonant spin component in Eq. (3) linear in $\lambda_{\rm so}$, $\delta\boldsymbol{s}_\omega = \delta s_k\hat{\boldsymbol{k}} + \delta s_\varphi\hat{\boldsymbol{\varphi}}$, is given by

$$\delta s_{k,\varphi}(\omega) = s^0\beta_{k,\varphi}\frac{2\hbar^{-1}\lambda_{\rm so}\Omega_k\mathcal{T}}{(\Omega_{\rm ex}^2 - \omega^2)(\Omega_k^2 - \omega^2)}, \tag{6}$$

where $\beta_{k,\varphi} = (\Omega_{\rm ex}, -i\omega)$ and $s^0 = \pm 1/2$ is the initial spin state. A pole at $\hbar\omega = \Delta$ corresponds to intersubband spin-flip transitions. This resonance contributes to the absorption, which can be calculated from Eq. (6) in the rotating frame [48] by collecting the spin response from all electrons with different quantum numbers [51].

We can complement this analysis by evaluating, quantum mechanically, the EDSR-induced absorption. The matrix element $M_{\uparrow\downarrow}$ of the direct intersubband spin-flip transition from $(+\downarrow)$ to $(+\uparrow)$ states (see Fig. 1) is found from the second-order perturbation theory

$$M_{\uparrow\downarrow} = \frac{\mathcal{V}_{(+\uparrow;-\uparrow)}\mathcal{H}^{\rm so}_{(-\uparrow;+\downarrow)}}{\varepsilon^+_{k,\downarrow} - \varepsilon^-_{k,\uparrow}} + \frac{\mathcal{H}^{\rm so}_{(+\uparrow;-\downarrow)}\mathcal{V}_{(-\downarrow;+\downarrow)}}{\varepsilon^+_{k,\downarrow} + \hbar\omega - \varepsilon^-_{k,\downarrow}}, \tag{7}$$

where $\varepsilon^{\pm}_{k,s} = \pm v_F\hbar k + s\Delta$ and $\mathcal{V} = \hbar\boldsymbol{\Omega}_{{\rm int},\omega}\cdot\boldsymbol{\tau}$. The spin-generation rate is given by Fermi's golden rule

$$W_s = \frac{2\pi}{\hbar}\sum_k 2|M_{\uparrow\downarrow}|^2(f_k^{\uparrow} - f_k^{\downarrow})\mathcal{L}(\hbar\omega), \tag{8}$$

where $f_k^{\uparrow,\downarrow}$ is the Fermi-Dirac function of $(\uparrow,\downarrow)$ electrons in the conduction band, the factor 2 accounts for (K, K') valleys, and the frequency broadening $\mathcal{L}(\hbar\omega) = (\gamma/\pi)/[(\hbar\omega - \Delta)^2 + \gamma^2]$ is given by the Lorentzian with the spin-flip dephasing rate, γ. We express $W_s = \alpha_{\rm sf}(\omega)(I/\hbar\omega)$ in terms of the radiation intensity, I, and the absorption coefficient, $\alpha_{\rm sf}(\omega)$, which at zero temperature is $\alpha_{\rm sf} = \pi\gamma\alpha^{\max}_{\rm sf}\mathcal{L}(\hbar\omega)$ with

$$\alpha^{\max}_{\rm sf} = \alpha_0 b\frac{\lambda^2_{\rm so}}{4\Delta\pi\gamma}\left[\ln\left(\frac{\mu+\Delta}{\mu-\Delta}\right) + \frac{\Delta^3/2\mu}{(\mu^2-\Delta^2)}\right], \tag{9}$$

where $b \sim 1$ is a prefactor determined by the directions of $\boldsymbol{\Delta}, \boldsymbol{E}_\omega$. The same expression for $\alpha_{\rm sf}(\omega)$ can be obtained using the Kubo formula for the optical conductivity by including SOC in the velocity matrix elements [51].

$\alpha^{\max}_{\rm sf}$ from Eq. (9) has an anomalous and counterintuitive polarization structure encoded in b, reflecting the role of both the pseudospin dynamics and SOC field symmetry for EDSR. Instead of directly interacting with $\boldsymbol{E}_\omega$, a K-valley electron spin interacts with a SOC field, $\hbar\boldsymbol{\Omega}_{\rm so}(t) = -2\lambda_{\rm so}\delta\tau_\varphi(t)\hat{\boldsymbol{k}}$ linearly polarized, irrespective of $\boldsymbol{E}_\omega$. For a gapless spectrum, this results in the suppressed EDSR sensitivity to the $\boldsymbol{E}_\omega$ polarization: for $\boldsymbol{\Delta} \parallel \hat{z}$, $\alpha_{\rm sf}$ is the same for both circular polarizations with $b = 1$, while, in the case of the in-plane $\boldsymbol{\Delta}$ orientation, $b = 3/4$ and $b = 1/4$, for $\boldsymbol{E} \parallel \boldsymbol{\Delta}$ and $\boldsymbol{E} \perp \boldsymbol{\Delta}$, respectively.

However, for massive Dirac electrons with $\mu \lesssim 2U$ the EDSR at $\boldsymbol{\Delta} \parallel \hat{z}$ and $\Delta > 0$ is induced preferably for σ^+ polarization, as shown in Fig. 3 for $\alpha^-_{\rm sf}/\alpha^+_{\rm sf}$. In contrast to Eq. (4), at $pv_F \ll U$ the vector $\boldsymbol{\tau}^0 \parallel \hat{z}$ and $\delta\boldsymbol{\tau}_\omega$ lies within the electron motion plane, implying $\boldsymbol{\Omega}_{\rm so}(t) \propto \lambda_{\rm so}[\hat{z}\times\hat{\boldsymbol{\rho}}_\sigma(t)]$ follows $\hat{\boldsymbol{\rho}}_\sigma(t)$, with the unit vector rotating counter- or clockwise depending on σ. Hence the spin resonance for $\delta\boldsymbol{s}_\omega$ obeys the ordinary polarization rules, i.e., at $\boldsymbol{\Omega}_{\rm ex} \parallel \hat{z}$, the EDSR absorption is active only for σ^+ in both valleys. As μ departs from the conduction band bottom, $\boldsymbol{\Omega}_k$ and $\boldsymbol{\tau}^0$ gradually tilt onto the plane, which suppresses the polarization sensitivity of the EDSR approaching the result $b = 1$ for the linear spectrum at $\mu \gg U$; see Fig. 3. This behavior also contrasts the valley-dependent circular dichroism for the interband spin-conserving absorption [58–60], i.e., the fundamental absorption in the $K(K')$ valley occurs for $\sigma^+(\sigma^-)$. A more accurate analysis [51] shows that at $\mu \lesssim U$ the EDSR does inherit a finite valley dependence with slightly different absorptions of σ^+ light in K and K' valleys.

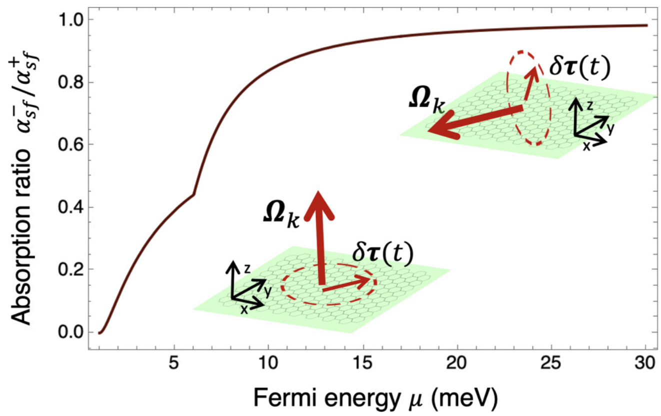

FIG. 3. Ratio of the EDSR absorption for two circular polarizations of $\boldsymbol{E}_\omega$ as a function of the Fermi energy. The parameters are $\Delta = 5$ meV, $\lambda_{\rm so} = 1.2$ meV, and $U = 3.5$ meV.

At smaller frequencies ∼GHz, $\omega\tau_p \lesssim 1$, there is a change in the mechanism for the EDSR resonance from Eqs. (2) and (3) to the current-induced spin resonance [37,47]. Here, a spin torque acting on a 2DEG equilibrium spin density $\boldsymbol{S}^0 = \boldsymbol{\Delta}/2\pi v_F^2\hbar^2$ stems from an effective Larmor frequency $\boldsymbol{\Omega}^{\rm D}_{\rm so}(t) = (\lambda_{\rm so}/\hbar v_F)[\hat{z}\times\boldsymbol{v}(t)]$, determined by the Drude velocity $\boldsymbol{v}(t) = 2\,{\rm Re}[\boldsymbol{v}_\omega e^{-i\omega t}]$ with $\boldsymbol{v}_\omega = e\boldsymbol{E}_\omega\tau(v_F/p_F)/(1 - i\omega\tau)$. One can qualitatively analyze the emerging nonequilibrium spin density, $\boldsymbol{S}_\omega$, based on the Bloch spin-resonance equation

$$-i\omega\boldsymbol{S}_\omega + T_2^{-1}\boldsymbol{S}_\omega = [\boldsymbol{\Omega}_{\rm ex}\times\boldsymbol{S}_\omega] + \left[\boldsymbol{\Omega}^{\rm D}_{{\rm so},\omega}\times\boldsymbol{S}^0\right]. \tag{10}$$

Since $\boldsymbol{\Omega}^{\rm D}_{{\rm so},\omega} \propto [\hat{z}\times\boldsymbol{E}_\omega]$, the resonant absorption for $\boldsymbol{\Delta} \parallel \hat{z}$ will be active only for one circular polarization. For the in-plane geometry, the absorption only takes place when $\boldsymbol{E} \parallel \boldsymbol{\Delta}$, since the torque is absent as $\boldsymbol{\Omega}^{\rm D}_{{\rm so},\omega} \parallel \boldsymbol{S}^0$ for $\boldsymbol{E} \perp \boldsymbol{\Delta}$. In the intermediate regime, $\omega\tau_p \sim 1$, both resonance mechanisms (intraband and intersubband) should be considered on equal footing.

It is instructive to compare $\alpha^{\max}_{\rm sf}$ with $\alpha_0 \approx 2.5\%$ for graphene. For $\mu \gtrsim 2\Delta$ (or $\mu \gtrsim 2U$ for massive Dirac electrons with $U > \Delta$) $\alpha_{\rm sf}(\omega) \approx \alpha_0 b(\lambda^2_{\rm so}/2\mu)\mathcal{L}(\hbar\omega)$, with the peak value determined by $\alpha^{\max}_{\rm sf} = \alpha_0 b\lambda^2_{\rm so}/(2\pi\mu\gamma)$. For $\mu = 16$ meV, $\lambda_{\rm so} = 0.7$ meV, and $T_2 = \hbar/\gamma = 70$ ps, we obtain $\alpha^{\max}_{\rm sf} \approx 0.55\alpha_0 = 1.25\%$. We also compare the EDSR-induced $M_{\uparrow\downarrow}$ from Eq. (7) with the matrix element of spin-flip transitions due to magnetodipole interaction, $M_{\rm md} = \mu_B g_e B/2$, where g_e is the electron g factor and B is the magnetic field. With $g_e \approx 1.99$ in graphene, $M_{\rm md}/M_{\uparrow\downarrow} \approx 10^{-4}$, giving a strong SOC enhancement of the spin susceptibility compared to the ESR.

Our results for the linear spectrum and $\alpha^{\max}_{\rm sf}(\mu)$ from Eq. (9) in Fig. 4(a) reveal an enhanced absorption when spin and pseudospin resonances approach each other at $\mu \to \Delta$. To analyze $\alpha_{\rm sf}(\omega)$ at $\mu \approx \Delta$, one needs to treat SOC nonperturbatively and account for spin-pseudospin correlations responsible for interband spin-flip transitions [61,62] at combined frequencies $(\Omega_k \pm \Omega_{\rm ex})$. We further identify an

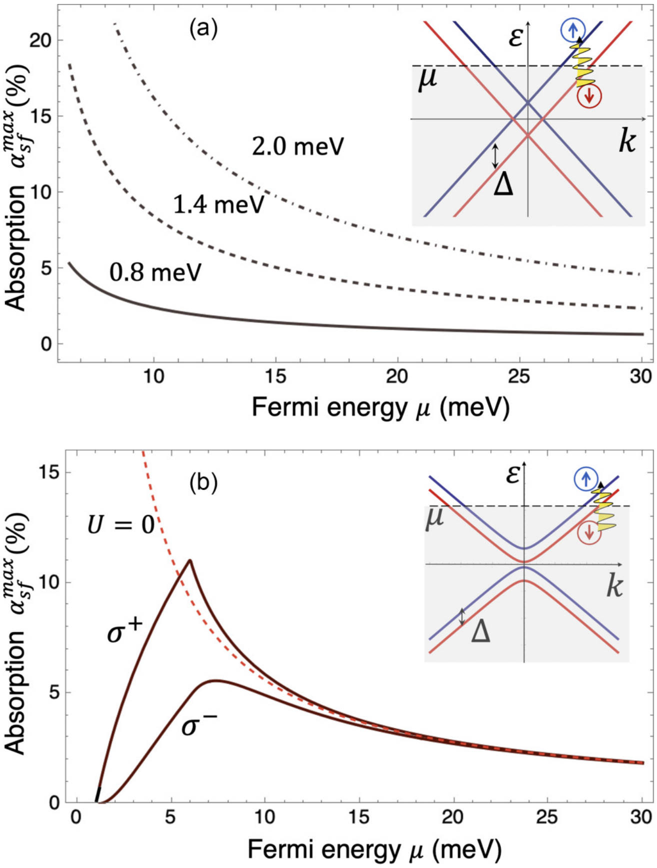

FIG. 4. Evolution of the spin-pseudospin coupling-induced EDSR absorption with the Fermi energy and SOC. (a) Linear spectrum (inset); the parameters are $\Delta = 5$ meV, $\hbar/\gamma = 70$ ps, with γ the spin-flip dephasing rate, and $\lambda_{\rm so} = 0.8,\ 1.4$, and 2.0 meV. (b) Massive Dirac electrons (inset) for two circular polarizations, $U = 3.5$ meV, and $\lambda_{\rm so} = 1.2$ meV.

enhanced spin-light coupling with SOC, as $\alpha_{\rm sf}^{\rm max} \propto \lambda_{\rm so}^2/\gamma$ from Eq. (9). For $\lambda_{\rm so} = 2$ meV and $\hbar/\gamma = 70$ ps, $\alpha_{\rm sf}^{\rm max} >$ 20%, an order of magnitude larger than α_0. $\alpha_{\rm sf}^{\rm max} \propto \lambda_{\rm so}^2/\gamma$ is sensitive to the spin relaxation rate [37,63], which might be suppressed by $\mathbf{\Delta}$ [64] (implying an enhanced EDSR efficiency), while also having an inherent anisotropy in graphene-based heterostructures [65,66]. For massive Dirac electrons and different $\boldsymbol{E}_\omega$ polarizations, $\alpha_{\rm sf}^{\rm max}(\mu)$ is shown in Fig. 4(b) [51]. $\alpha_{\rm sf}^{\rm max}$ maximum at $\mu \approx U/2$ has the magnitude still larger than ESR. For both cases, $\alpha_{\rm sf}^{\rm max}$ decreases at $\mu \gg \Delta$ due to dynamic suppression of spin-pseudospin coupling; see the denominator of $\delta\boldsymbol{\tau}_\omega$, $\delta\boldsymbol{s}_\omega$ in Eqs. (4) and (6).

As an alternative to spectroscopic studies, we propose the electrical detection of resonant spin generation by THz radiation [51]. This is based on interfacial spin-to-charge conversion at the graphene-ferromagnet (F) contact. With the proximity-induced Δ in graphene and the spin-dependent interfacial properties, together with the common μ and charge transfer, the THz absorption in graphene leads to a nonequilibrium spin polarization and the generation of an interfacial electromotive force (EMF). This scheme is an extension of the Johnson-Silsbee spin-charge coupling or spin-voltaic effect [36,67–70] applied to Dirac materials, where EMF can be detected electrically. To preserve graphene's Dirac spectrum, in addition to an insulating or metallic F with h-BN spacer [21,71], even a direct contact with a metallic F can be suitable [22]. The enhanced spin-to-charge interconversion at the graphene-F interfaces enables THz optospintronics and graphene THz detection.

We have revealed the role of coupled spin-pseudospin dynamics for the understanding of THz spin susceptibility in proximitized Dirac materials. The discovered features are universal for a wide range of vdW heterostructures: (i) graphene with proximity-induced Zeeman spin splitting by various magnetic substrates [22–25,72–80], (ii) vdW hexagonal crystals with gapped spectrum, such as silicene [81], Bi(111) [82], or puckered 2D lattice with Dirac points [83], and (iii) nonmagnetic bilayers, such as graphene/TMD [8,10,11], with valley-dependent Zeeman spin splitting due to the hybridization of graphene p states with TMD bands [4,8,10]. In the latter case, we predict that, for $\mu \lesssim 2U$ and $B = 0$, the EDSR will be induced selectively for K or K', depending on the circular polarization. Furthermore, EDSR in graphene/TMD can imprint many-body effects from collective modes of spin-orbital Fermi liquids [62,84].

With challenges and experimental surprises in the understanding of Zeeman splitting [85,86], a key parameter in proximitized vdW heterostructures, EDSR studies offer a versatile probe to address this situation and to quantify other proximity-induced spin splittings. For instance, our predicted polarization structure of $\alpha_{\rm sf}$, with its small-μ enhancement, has a clear difference as compared to k-linear SOC. In that case, for the spin-light coupling, $\boldsymbol{k} \to \boldsymbol{k} - (e/c)\boldsymbol{A}$ in the $\boldsymbol{k}$-linear Rashba Hamiltonian, $H_{\rm R} = \lambda_{\rm R}(\boldsymbol{k} \times \hat{\boldsymbol{z}})\boldsymbol{s}$, leads to the interaction potential, $\mathcal{V}' = e\lambda_{\rm R}(\hat{\boldsymbol{z}} \times \boldsymbol{A}_\omega)\boldsymbol{s}/c$, that couples $\boldsymbol{A}_\omega$ directly with the electron spin, rather than with pseudospin. For the usual SOC strength, $\lambda_{\rm R}$, the corresponding torque leads to spin-flip transitions in $\mathbf{\Delta}$ with an ordinary polarization structure. As a fingerprint for different contributions to spin-light coupling in proximitized Dirac materials, it is natural to analyze the polarization dependence of EDSR for different mutual orientations of $\mathbf{\Delta}$, $\boldsymbol{E}_\omega$, and its μ dependence.

The phenomenon of a coupled spin-pseudospin dynamics has a broad range of implications beyond the EDSR, as it is inherent to many other manifestations of the spin-charge conversion, such as the spin-voltaic or spin-galvanic effects [69,87], which can be strongly modified in Dirac systems and whose dynamical properties remain to be understood. Another striking example is the study of the spin-orbit torque (SOT), which is expected to enable the next generation of embedded memories using 2D materials or to integrate photonics, electronics, and spintronics [88–90]. However, the spin-pseudospin dynamics in SOT has not been explored. With the push towards ultrafast SOT [91], our analysis of the THz spin-charge conversion, provides a further motivation to consider proximitized vdW heterostuctures, both for the resonant SOT generation and for the THz spintronics beyond magnetic multilayers.

Our picture could be used to analyze nonlinear optical response of Dirac systems and the nonlinear Hall effect [92] for different topological regimes [93]. The inverse effect of spin precession on orbital dynamics can be derived from the coupled spin-pseudospin dynamics, providing an alternative treatment of the topology-sensitive Kerr effect [94,95]. The discussed picture could be also used to analyze spin-flip transitions in a Dirac system with a stronger SOC, such as graphene-TMD heterostructures [4], and be implemented in graphene quantum dots and nanoflakes to realize qubits for THz quantum computing. While SOC has been employed to realize fast qubit rotations and control with electric fields [39,42,43], EDSR has not been exploited in graphene or bilayer graphene due to their low intrinsic SOC [96].

We thank K. Y. Golenitskii for discussing optical properties of magnetic vdW heterostructures, B. D. McCombe for discussing the EDSR history, and D. Torres (ICN2) for help with 3D device models in Figs. 1 and 2. Analytical work at Ioffe Institute by K.S.D. was supported by the Russian Science Foundation (RSF), Project No. 22-22-20082 (RSF Contract No. 22-22-20082 from 25.03.2022; contract with a regional Grant No. 23/2022 from 14.04.2022). I.Ž. was supported by the U.S. DOE, Office of Science BES, Award No. DE-SC0004890. S.O.V. was supported by the Spanish Ministry of Science and Innovation (MCIN) and the Spanish Research Agency (MCIN/AEI/10.13039/501100011033) through Grants No. PID2019-111773RB-I00 and No. PID2022-143162OB-I00 and Severo Ochoa CEX2021-001214-S. I.V.R. acknowledges Council for At-Risk Academics (CARA) support.

[1] A. K. Geim and I. V. Grigorieva, van der Waals heterostructures, Nature (London) **499**, 419 (2013).

[2] K. S. Novoselov, O. A. Mishchenko, O. A. Carvalho, and A. H. Castro Neto, 2D materials and van der Waals heterostructures, Science **353**, aac9439 (2016).

[3] I. Žutić, A. Matos-Abiague, B. Scharf, H. Dery, and K. Belashchenko, Proximitized materials, Mater. Today **22**, 85 (2019).

[4] J. F. Sierra, J. Fabian, R. K. Kawakami, S. Roche, and S. O. Valenzuela, Van der Waals heterostructures for spintronics and opto-spintronics, Nat. Nanotechnol. **16**, 856 (2021).

[5] W. Han, R. K. Kawakami, M. Gmitra, and J. Fabian, Graphene spintronics, Nat. Nanotechnol. **9**, 794 (2014).

[6] W. Han, Perspectives for spintronics in 2D materials, APL Mater. **4**, 032401 (2016).

[7] A. Avsar, H. Ochoa, F. Guinea, B. Özyilmaz, B. J. van Wees, and I. J. Vera-Marun, Colloquium: Spintronics in graphene and other two-dimensional materials, Rev. Mod. Phys. **92**, 021003 (2020).

[8] M. Gmitra and J. Fabian, Graphene on Transition-metal dichalcogenides: A platform for proximity spin-orbit physics and optospintronics, Phys. Rev. B **92**, 155403 (2015).

[9] M. Gmitra, D. Kochan, P. Högl, and J. Fabian, Trivial and inverted Dirac bands and the emergence of quantum spin Hall states in graphene on transition-metal dichalcogenides, Phys. Rev. B **93**, 155104 (2016).

[10] J. H. Garcia, M. Vila, A. W Cummings, and S. Roche, Spin transport in graphene/transition metal dichalcogenide heterostructures, Chem. Soc. Rev. **47**, 3359 (2018).

[11] A. David, P. Rakyta, A. Kormányos, and G. Burkard, Induced spin-orbit coupling in twisted graphene–transition metal dichalcogenide heterobilayers: Twistronics meets spintronics, Phys. Rev. B **100**, 085412 (2019).

[12] A. W. Cummings, J. H. Garcia, J. Fabian, and S. Roche, Anisotropy in graphene induced by proximity effects, Phys. Rev. Lett. **119**, 206601 (2017).

[13] L. A. Benítez, J. F. Sierra, W. Savero Torres, A. Arrighi, F. Bonell, M. V. Costache, and S. O. Valenzuela, Strongly anisotropic spin relaxation in graphene/transition metal dichalcogenide heterostructures at room temperature, Nat. Phys. **14**, 303 (2018).

[14] T. S. Ghiasi, J. Ingla-Aynés, A. A. Kaverzin, and B. J. van Wees, Induced spin lifetime anisotropy in transition metal dichalcogenide/graphene, Nano Lett. **17**, 7528 (2017).

[15] M. Offidani, M. Milletarì, R. Raimondi, and A. Ferreira, Optimal charge-to-spin conversion in graphene on transition-metal dichalcogenides, Phys. Rev. Lett. **119**, 196801 (2017).

[16] J. H. Garcia, A. W. Cummings, and S. Roche, Spin Hall effect and weak antilocalization in graphene/transition metal dichalcogenide heterostructures, Nano Lett. **17**, 5078 (2017).

[17] C. K. Safeer, J. Ingla-Aynés, F. Herling, J. H Garcia, M. Vila, N. Ontoso, M. R. Calvo, S. Roche, L. E. Hueso, and F. Casanova, Room-temperature spin Hall effect in graphene/MoS_2 van der Waals heterostructures, Nano Lett. **19**, 1074 (2019).

[18] L. A. Benítez, W. Savero Torres, J. F. Sierra, M. Timmermans, J. H. Garcia, S. Roche, M. V. Costache, and S. O. Valenzuela, Tunable room-temperature spin galvanic and spin Hall effects in van der Waals heterostructures, Nat. Mater. **19**, 170 (2020).

[19] R. Galceran, B. Tian, J. Li, F. Bonell, M. Jamet, C. Vergnaud, A. Marty, J. H. García, J. F. Sierra, M. V. Costache *et al.*, Control of spin-charge conversion in van der Waals heterostructures, APL Mater. **9**, 100901 (2021).

[20] H. X. Yang, A. Hallal, D. Terrade, X. Waintal, S. Roche, and M. Chshiev, Proximity effects induced in graphene by magnetic insulators: First-principles calculations on spin filtering and exchange-splitting gaps, Phys. Rev. Lett. **110**, 046603 (2013).

[21] P. Lazić, K. D. Belashchenko, and I. Žutić, Effective gating and tunable magnetic proximity effects in two-dimensional heterostructures, Phys. Rev. B **93**, 241401(R) (2016).

[22] P. U. Asshoff, J. L. Sambricio, A. P. Rooney, S. Slizovskiy, A. Mishchenko, A. M. Rakowski, E. W. Hill, A. K. Geim, S. J. Haigh, V. I. Fal'ko *et al.*, Magnetoresistance of vertical Co-graphene-NiFe junctions controlled by charge transfer and proximity-induced spin splitting in graphene, 2D Mater. **4**, 031004 (2017).

[23] P. Wei, S. Lee, F. Lemaitre, L. Pinel, D. Cutaia, W. Cha, F. Katmis, Y. Zhu, D. Heiman, J. Hone *et al.*, Strong interfacial exchange field in the graphene/EuS heterostructure, Nat. Mater. **15**, 711 (2016).

[24] Y. Wu, G. Yin, L. Pan, A. J. Grutter, Q. Pan, A. Lee, D. A. Gilbert, J. A. Borchers, W. Ratcliff, A. Li *et al.*, Large exchange splitting in monolayer graphene magnetized by an antiferromagnet, Nat. Electron. **3**, 604 (2020).

[25] T. S. Ghiasi, A. A. Kaverzin, A. H. Dismukes, D. K. de Wal, X. Roy, and B. J. van Wees, Electrical and thermal generation of spin currents by magnetic bilayer graphene, Nat. Nanotechnol. **16**, 788 (2021).

[26] H. Wen, H. Dery, W. Amamou, T. Zhu, Z. Lin, J. Shi, I. Žutić, I. Krivorotov, L. J. Sham, and R. K. Kawakami, Experimental demonstration of XOR operation in graphene magnetologic gates at room temperature, Phys. Rev. Appl. **5**, 044003 (2016).

[27] S. Castilla, B. Terrés, M. Autore, L. Viti, J. Li, A. Y. Nikitin, I. Vangelidis, K. Watanabe, T. Taniguchi, E. Lidorikis *et al.*, Fast and sensitive terahertz detection using an antenna-integrated graphene pn junction, Nano Lett. **19**, 2765 (2019).

[28] H. A. Hafez, S. Kovalev, K. Tielrooij, M. Bonn, M. Gensch, and D. Turchinovich, Terahertz nonlinear optics of graphene: From saturable absorption to high-harmonics generation, Adv. Opt. Mater. **8**, 1900771 (2020).

[29] S. Kovalev, H. A. Hafez, K. Tielrooij, J. Deinert, I. Ilyakov, N. Awari, D. Alcaraz, K. Soundarapandian, D. Saleta, S. Germanskiy *et al.*, Electrical tunability of terahertz nonlinearity in graphene, Sci. Adv. **7**, eabf9809 (2021).

[30] K.-J. Tielrooij, A. Principi, D. S. Reig, A. Block, S. Varghese, S. Schreyeck, K. Brunner, G. Karczewski, I. Ilyakov, O. Ponomaryov *et al.*, Milliwatt terahertz harmonic generation from topological insulator metamaterials, Light: Sci. Appl. **11**, 315 (2022).

[31] E. I. Rashba, Properties of semiconductors with an extremum loop. I. Cyclotron and combinational resonance in a magnetic field perpendicular to the plane of the loop, Sov. Phys. Solid State **2**, 1109 (1960).

[32] E. I. Rashba, Spintronics: sources and challenge, J. Supercond. **15**, 13 (2002).

[33] R. L. Bell, Electric dipole spin transitions in InSb, Phys. Rev. Lett. **9**, 52 (1962).

[34] B. D. McCombe, S. G. Bishop, and R. Kaplan, Combined resonance and electron *g* values in InSb, Phys. Rev. Lett. **18**, 748 (1967).

[35] S. I. Pekar and E. I. Rashba, Combined resonance in crystals in inhomogeneous magnetic field, Sov. Phys. JETP **20**, 1295 (1965).

[36] I. Žutić, J. Fabian, and S. Das Sarma, Spintronics: Fundamentals and applications, Rev. Mod. Phys. **76**, 323 (2004).

[37] M. Duckheim and D. Loss, Electric-dipole-induced spin resonance in disordered semiconductors, Nat. Phys. **2**, 195 (2006).

[38] Z. Wilamowski, W. Ungier, and W. Jantsch, Electron spin resonance in a two-dimensional electron gas induced by current or by electric field, Phys. Rev. B **78**, 174423 (2008).

[39] S. Nadj-Perge, S. M. Frolov, P. A. M. Bakkers, and L. P. Kouwenhoven, Spin-orbit qubit in a semiconductor nanowire, Nature (London) **468**, 1084 (2010).

[40] A. V. Stier, C. J. Meining, V. R. Whiteside, B. D. McCombe, E. I. Rashba, P. Grabs, and L. W. Molenkamp, Electric-dipole spin resonance and spin-orbit coupling effects in odd-integer quantum Hall edge channels, Phys. Rev. B **107**, 045301 (2023).

[41] M. Brooks and G. Burkard, Electric dipole spin resonance of two-dimensional semiconductor spin qubits, Phys. Rev. B **101**, 035204 (2020).

[42] K. Wang, G. Xu, F. Gao, He Liu, R.-L. Ma, X. Zhang, Z. Wang, G. Cao, T. Wang, J.-J. Zhang *et al.*, Ultrafast coherent control of a hole spin qubit in a germanium quantum dot, Nat. Commun. **13**, 206 (2022).

[43] P. Stano and D. Loss, Review of performance metrics of spin qubits in gated semiconducting nanostructures, Nat. Rev. Mater. **4**, 672 (2022).

[44] D. van Tuan, F. Ortmann, D. Soriano, S. O. Valenzuela, and S. Roche, Pseudospin-driven spin relaxation mechanism in graphene, Nat. Phys. **10**, 857 (2014).

[45] B. G. de Moraes, A. W. Cummings, and S. Roche, Emergence of intraparticle entanglement and time-varying violation of Bell's inequality in Dirac matter, Phys. Rev. B **102**, 041403(R) (2020).

[46] M. Duckheim and D. Loss, Resonant spin polarization and spin current in a two-dimensional electron gas, Phys. Rev. B **75**, 201305(R) (2007).

[47] Z. Wilamowski, H. Malissa, F. Schäffler, and W. Jantsch, *g*-Factor tuning and manipulation of spins by an electric current, Phys. Rev. Lett. **98**, 187203 (2007).

[48] J. A. Weil and J. R. Bolton, *Electron Paramagnetic Resonance: Elementary Theory and Practical Applications* (John Wiley & Sons, New York, 2007).

[49] E. I. Rashba and Al. L. Efros, Efficient electron spin manipulation in a quantum well by an in-plane electric field, Appl. Phys. Lett. **83**, 5295 (2003).

[50] P. Kim, Graphene and Relativistic Quantum Physics, in *Dirac Matter*, edited by B. Duplantier, V. Rivasseau, and J.-N. Fuchs (Springer International Publishing, Cham, 2017), pp. 1–23.

[51] See Supplemental Material at http://link.aps.org/supplemental/10.1103/PhysRevB.109.L201406 for expanded discussion of theoretical and computational methods, which includes Refs. [52,53].

[52] K. Nomura and A. H. MacDonald, Quantum transport of massless Dirac fermions, Phys. Rev. Lett. **98**, 076602 (2007).

[53] S. Barati and S. H. Abedinpour, Optical conductivity of three and two dimensional topological nodal-line semimetals, Phys. Rev. B **96**, 155150 (2017).

[54] J. J. Sakurai and J. Napolitano, *Modern Quantum Mechanics*, 2nd ed. (Addison-Wesley, San Francisco, 2011), p. 342.

[55] D. J. Griffiths, *Introduction to Quantum Mechanics*, 2nd ed. (Prentice Hall, Upper Saddle River, NJ, 2018), p. 178.

[56] M. Gmitra, S. Konschuh, C. Ertler, C. Ambrosch-Draxl, and J. Fabian, Band-structure topologies of graphene: Spin-orbit coupling effects from first principles, Phys. Rev. B **80**, 235431 (2009).

[57] H. Min, J. E. Hill, N. A. Sinitsyn, B. R. Sahu, L. Kleinman, and A. H. MacDonald, Intrinsic and Rashba spin-orbit interactions in graphene sheets, Phys. Rev. B **74**, 165310 (2006).

[58] T. Cao, G. Wang, W. Han, H. Ye, C. Zhu, J. Shi, Q. Niu, P. Tan, E. Wang, and B. Liu, Valley-selective circular dichroism of monolayer molybdenum disulphide, Nat. Commun. **3**, 887 (2012).

[59] K. F. Mak, K. He, J. Shan, and T. F. Heinz, Control of valley polarization in monolayer MoS_2 by optical helicity, Nat. Nanotechnol. **7**, 494 (2012).

[60] D. Xiao, G. B. Liu, W. Feng, X. Xu, and W. Yao, Coupled spin and valley physics in monolayers of MoS_2 and other group-VI dichalcogenides, Phys. Rev. Lett. **108**, 196802 (2012).

[61] M. Inglot, V. K. Dugaev, E. Ya. Sherman, and J. Barnaś, Optical spin injection in graphene with Rashba spin-orbit interaction, Phys. Rev. B **89**, 155411 (2014).

[62] A. Kumar, S. Maiti, and D. L. Maslov, Zero-field spin resonance in graphene with proximity-induced spin-orbit coupling, Phys. Rev. B **104**, 155138 (2021).

[63] M. Offidani, R. Raimondi, and A. Ferreira, Microscopic linear response theory of spin relaxation and relativistic transport phenomena in graphene, Conden. Matter **3**, 18 (2018).

[64] M. W. Wu, J. H. Jiang, and M. Q. Weng, Spin dynamics in semiconductors, Phys. Rep. **493**, 61 (2010).
[65] B. Raes, J. E. Scheerder, M. V. Costache, F. Bonell, J. F. Sierra, J. Cuppens, J. Van de Vondel, and S. O. Valenzuela, Determination of the spin-lifetime anisotropy in graphene using oblique spin precession, Nat. Commun. **7**, 11444 (2016).
[66] B. Raes, A. W. Cummings, F. Bonell, M. V. Costache, J. F. Sierra, S. Roche, and S. O. Valenzuela, Spin precession in anisotropic media, Phys. Rev. B **95**, 085403 (2017).
[67] R. H. Silsbee, Novel method for the study of spin transport in conductors, Bull. Magn. Reson. **2**, 284 (1980).
[68] M. Johnson and R. H. Silsbee, Interfacial charge-spin coupling: Injection and detection of spin magnetization in metals, Phys. Rev. Lett. **55**, 1790 (1985).
[69] I. Žutić, J. Fabian, and S. Das Sarma, Spin-polarized transport in inhomogeneous magnetic semiconductors: Theory of magnetic/nonmagnetic *p-n* junctions, Phys. Rev. Lett. **88**, 066603 (2002).
[70] J. Fabian, A. Matos-Abiague, C. Ertler, P. Stano, and I. Žutić, Semiconductor spintronics, Acta Phys. Slov. **57**, 565 (2007).
[71] J. Xu, S. Singh, J. Katoch, G. Wu, T. Zhu, I. Žutić, and R. K. Kawakami, Spin inversion in graphene spin valves by gate-tunable magnetic proximity effect at one-dimensional contacts, Nat. Commun. **9**, 2869 (2018).
[72] A. Dahal and M. Batzill, Graphene-nickel interfaces: a review, Nanoscale **6**, 2548 (2014).
[73] M. Cattelan, G. W. Peng, E. Cavaliere, L. Artiglia, A. Barinov, L. T. Roling, M. Favaro, I. Pis, S. Nappini, E. Magnano *et al.*, The nature of the Fe-graphene interface at the nanometer level, Nanoscale **7**, 2450 (2015).
[74] W. Q. Liu, W. Y. Wang, J. J. Wang, F. Q. Wang, C. Lu, F. Jin, A. Zhang, Q. M. Zhang, G. Laan, Y. B. Xu *et al.*, Atomic-scale interfacial magnetism in Fe/graphene heterojunction, Sci. Rep. **5**, 11911 (2015).
[75] A. G. Swartz, P. M. Odenthal, Y. Hao, R. S. Ruoff, and R. K. Kawakami, Integration of the ferromagnetic insulator EuO onto graphene, ACS Nano **6**, 10063 (2012).
[76] Z. Wang, C. Tang, R. Sachs, Y. Barlas, and J. Shi, Proximity-induced ferromagnetism in graphene revealed by the anomalous Hall effect, Phys. Rev. Lett. **114**, 016603 (2015).
[77] K. Zollner, M. D. Petrović, K. Dolui, P. Plecháč, B. K. Nikolić, and J. Fabian, Scattering-induced and highly tunable by gate damping-like spin-orbit torque in graphene doubly proximitized by two-dimensional magnet $Cr_2Ge_2Te_6$ and monolayer WS_2, Phys. Rev. Res. **2**, 043057 (2020).
[78] C. Tang, Z. Zhang, S. Lai, Q. Tan, and W. Gao, Magnetic proximity effect in graphene/$CrBr_3$ van der Waals heterostructures, Adv. Mater. **32**, 1908498 (2020).
[79] B. Zhou, S. Ji, Z. Tian, W. Cheng, X. Wang, and W. Mi, Proximity effect induced spin filtering and gap opening in graphene by half-metallic monolayer Cr_2C ferromagnet, Carbon **132**, 25 (2018).
[80] M. U. Farooq and J. Hong, Switchable valley splitting by external electric field effect in graphene/CrI_3 heterostructures, npj 2D Mater. Appl. **3**, 3 (2019).
[81] A. Kara, H. Enriquez, A. P. Seitsonen, L. C. Lew Yan Voon, S. Vizzini, B. Aufray, and H. Oughaddou, A review on silicene — New candidate for electronics, Surf. Sci. Rep. **67**, 1 (2012).
[82] F. Reis, G. Li, L. Dudy, M. Bauernfeind, S. Glass, W. Hanke, R. Thomale, J. Schäfer, and R. Claessen, Bismuthene on a SiC substrate: A candidate for a high-temperature quantum spin Hall material, Science **357**, 287 (2017).
[83] Y. Lu, D. Zhou, G. Chang, S. Guan, W. Chen, Y. Jiang, J. Jiang, X. Wang, S. A. Yang, and Y. P. Feng, Multiple unpinned Dirac points in group-Va single-layers with phosphorene structure, npj Comput. Mater. **2**, 16011 (2016).
[84] D. L. Maslov, A. Kumar, and S. Maiti, Collective spin modes in Fermi liquids with spin-orbit coupling, JETP **135**, 549 (2022).
[85] J. Choi, C. Lane, J.-X. Zhu, and S. A. Crooker, Asymmetric magnetic proximity interactions in $MoSe_2/CrBr_3$ van der Waals heterostructures, Nat. Mater. **22**, 305 (2023).
[86] T. Zhou and I. Žuté, Asymmetry in the magnetic neighbourhood, Nat. Mater. **22**, 284 (2023).
[87] S. D. Ganichev, E. L. Ivchenko, V. V. Bel'Kov, S. A. Tarasenko, M. Sollinger, D. Weiss, W. Wegscheider, and W. Prettl, Spin-galvanic effect, Nature (London) **417**, 153 (2002).
[88] H. Yang, S. O. Valenzuela, M. Chshiev, S. Couet, B. Dieny, B. Dlubak, A. Fert, K. Garello, M. Jamet, D.-E. Jeong *et al.*, Two-dimensional materials prospects for non-volatile spintronic memories, Nature (London) **606**, 663 (2022).
[89] P. A. Dainone, P. Renucci, A. Bouche, N. F. Prestes, M. Morassi, X. Devaux, M. Lindemann, J.-M. George, H. Jaffres, A. Lemaitre *et al.*, Controlling the helicity of light by electrical magnetization switching, Nature **627**, 783 (2024).
[90] E. Y. Tsymbal and I. Žutić, *Spintronics Handbook Spin Transport and Magnetism*, 2nd ed. (CRC Press, Taylor and Francis, Boca Raton, FL, 2012).
[91] K. Jhuria, J. Hohlfeld, A. Pattabi, E. Martin, A. Y. Arriola Córdova, X. Shi, R. Lo Conte, S. Petit-Watelot, J. C. Rojas-Sanchez, G. Malinowski *et al.*, Spin-orbit torque switching of a ferromagnet with picosecond electrical pulses, Nat. Electron. **3**, 680 (2020).
[92] I. Sodemann and L. Fu, Quantum nonlinear Hall effect induced by Berry curvature dipole in time-reversal invariant materials, Phys. Rev. Lett. **115**, 216806 (2015).
[93] R. K. Malla, A. Saxena, and W. J. M. Kort-Kamp, Emerging nonlinear Hall effect in Kane-Mele two-dimensional topological insulators, Phys. Rev. B **104**, 205422 (2021).
[94] K. S. Denisov, Electric field effect on electron gas spins in two-dimensional magnets with strong spin-orbit coupling, Phys. Rev. B **105**, 045413 (2022).
[95] Y. Yao, L. Kleinman, A. H. MacDonald, J. Sinova, T. Jungwirth, D. S. Wang, E. Wang, and Q. Niu, First principles calculation of anomalous Hall conductivity in ferromagnetic BCC Fe, Phys. Rev. Lett. **92**, 037204 (2004).
[96] C. Bray, K. Maussang, C. Consejo, J. A. Delgado-Notario, S. Krishtopenko, I. Yahniuk, S. Gebert, S. Ruffenach, K. Dinar, E. Moench *et al.*, Temperature-dependent zero-field splittings in graphene, Phys. Rev. B **106**, 245141 (2022).